Boosting hydrogen storage capacity in modified-graphdiyne structures: A comprehensive density functional study

M. Asgari Bajgirani, Z. Biglari, Mehdi Sahihi

Boosting Hydrogen Storage Capacity in Modified-Graphdiyne Structures: A Comprehensive Density Functional Study

M. Asgari Bajgirani[a], Z. Biglari[a]*, M. Sahihi[b,]*

[a] *Department of Physical Chemistry, Faculty of Chemistry, Lorestan University, Lorestan, Iran*

[b] *Université Clermont Auvergne, CNRS, Clermont Auvergne INP, Institut de Chimie de Clermont-Ferrand, F-63000 Clermont-Ferrand, France*

***Corresponding authors**

Zeinab Biglari and Mehdi Sahihi

Email: biglari.z@lu.ac.ir, ORCID ID: 0000-0003-1874-7041

Email: mehdi.sahihi@uca.fr, Tel.: +33 (0) 473407384

Abstract

Graphdiyne (GDY) is a recently discovered two-dimensional carbon allotrope that holds significant promise for applications in hydrogen adsorption and storage technology. This study investigates the impact of nitrogen doping and sodium decoration on the hydrogen adsorption capacity of GDY nanosheets while examining their influence on electronic and structural properties. Various deliberate impurities are introduced to create modified-GDY structures.

Nitrogen doping triggers a transition from a semiconductor to a semi-metallic state, driven by differences in electronegativity and adjustments in bond lengths. Cohesive energy (E_{coh}) is found to be -7.231 eV for the most stable N-doped GDY. In contrast, sodium decoration enhances conduction by modifying charge distribution. The other most stable structures are Na-decorated GDY with E_{ads} of -3.804 eV and N, Na-decorated GDY with -3.347 eV. Modified-GDY structures exhibit higher hydrogen adsorption energies compared to pristine GDY, with N-doped GDY displaying the highest energy levels (E_{ads} = -0.455eV). Maximum hydrogen adsorption capacities are assessed for each structure, and a notable improvement is observed in Na-decorated GDY (19 H_2), significantly enhancing the storage capacity to 13.8 wt%, which shows a 10.21 wt% increase in H_2 adsorption compared to pure GDY (3.59 wt%).

These findings underscore the potential of modified-GDY for hydrogen storage applications, highlighting the effectiveness of structural carbon modification in enhancing hydrogen adsorption capacity.

Keywords: Graphdiyne, Hydrogen Storage, Adsorption, Nitrogen Doping, Sodium Decoration, Density Functional Theory.

1. Introduction

In the present era of industrial expansion, the growing concern about greenhouse gas emissions underscores the need for a deeper exploration of sustainable energy sources as alternative solutions. It is imperative to adopt innovative approaches that can mitigate environmental pollution, ensuring a sustainable future for generations to come [1]. Hydrogen (H_2) has emerged as a promising energy carrier due to its clean properties, abundance, efficiency, eco-friendliness, and economic sustainability [2]. However, the challenge of developing a compact and efficient hydrogen storage system under ambient pressure conditions remains a significant obstacle to achieving energy-efficient hydrogen-based energy generation [3].

In recent years, a wide array of materials, including nonporous solid media, has been rapidly developed for use in hydrogen storage technologies [4]. Two-dimensional (2D) carbon-based materials, such as graphene and its derivatives [5–7], have shown promise for H_2 storage due to their high storage efficiency, as well as their chemical and thermal stability during the hydrogen adsorption-desorption process [8,9]. Nevertheless, research findings have indicated that pristine structures generally exhibit weak interactions with hydrogen, resulting in low storage capacity [10,11]. Consequently, it becomes imperative to modify these structures to enhance their interaction power and storage capacity, similar to the successful trapping of CO_2 gas [12,13].

Modifying nanomaterials by doping nonmetals or decorating metals is a common method to increase efficiency in this domain [14]. 2D and 3D graphite systems containing heteroatoms such as N, S, P, etc., can modify the thermal, mechanical, electronic, photonic, and surface properties of the material. In this regard, energy devices made using robust N-doped structures are very efficient in operation and very effective compared to pure systems [15]. Also, the strategy of introducing diffuse excess electrons has been proposed to design new type of high-

performance materials based on molecules, even extending to carbon nanostructures. One of these methods that leads to reducing the band gap and increasing the conductivity is decorating the structures with alkali metals [16]. In the meantime, sodium (Na) has been chosen due to its abundance and cost-effectiveness. In several studies, other metal and non-metal atoms like Al, Ga, Mg, Zn, S, and B have been used as dopants on the structures of carbon nanotubes (CNT), C60 and ZnO nanoparticles, and interesting results have been observed [17–20]. A recent study on boron-substituted zeolite templated carbon vacancies for hydrogen adsorption found that sodium decoration showed the best performance, allowing up to fifteen hydrogen molecules to be adsorbed with a 6.55% wt storage capacity [21]. The Density Functional Theory (DFT) method was employed to investigate the hydrogen storage potential of recently developed graphene nanoflakes doped with chromium (Cr) atoms. Unlike pure graphene nanoflakes, where H_2 molecules tended to migrate away from the surface, the Cr-doped graphene nanoflakes exhibited a strong attraction to H_2, as indicated by a chemical adsorption energy of -0.574 eV [22].

DFT calculations revealed that Mg-decorated graphyne, a graphene-based material, can effectively store up to ten hydrogen molecules under the influence of an electric field. This results in a remarkable hydrogen storage capacity of 10.64 wt% and an average adsorption energy of -0.28 eV per H_2 molecule [23]. Akbari et al. investigated the impact of Al or N atom doping on the electronic and structural properties of graphyne through DFT calculations [24]. Their study revealed that the introduction of these atoms altered the conductive nature of graphyne from a semiconductor to a metallic state. According to their findings, these materials can adsorb 4, 9, 7, and 16 H_2 molecules, respectively. Moreover, the hydrogen storage capacity of Al-N co-doped graphyne can attain an impressive 16.67 wt%.

In 2010, Li et al. achieved the successful synthesis of graphdiyne (GDY) for the first time by employing hexaethynyl benzene in a cross-coupling reaction on the surface of a copper (Cu)

foil [25]. GDY is a carbon allotrope consisting of hexagonal carbon rings connected by a diacetylene bridge (-C≡C-C≡C-). Its structure encompasses sp and sp^2 hybridized carbon atoms, with the sp–sp^2 hybridized carbon atoms serving as active sites [26]. Due to its unique physicochemical properties, GDY has garnered significant attention for various applications, spanning electronics, energy storage, electrode materials, lithium-ion batteries, photocatalysis, drug delivery, CO_2 capture, and hydrogen purification [27–32].

As with other structures, several methods have been proposed in the literature to enhance the reversible hydrogen storage capacity of GDY, including doping, decorating, and applying an electric field [33,34]. For instance, Jiao et al. investigated nitrogen-modified GDY and its potential for hydrogen purification from a CH_4/CO/H_2 mixture using DFT-D [29]. Their findings indicated that nitrogen doping enhances hydrogen purification capabilities by reducing the H_2 diffusion barrier and increasing the CH_4/CO diffusion barrier.

The addition of metal atoms to GDY can transform it from a small band-gap semiconductor to a metallic state, with metal atoms in a partially positive state being desirable for reversible H_2 storage materials. Panigrahi et al. conducted a study on GDY decorated with light metals such as Li, Na, K, Ca, Sc, and Ti (using the DFT-D3 method) to assess their potential for improving reversible hydrogen storage capacity. They observed a capacity of 6.50 wt% for double metal-decorated GDY [2]. The performance of Ca-decorated GDY in hydrogen storage was evaluated using DFT-D2. According to this research, Ca-decorated GDY can adsorb 14 H_2 molecules on each side of GDY with an average binding energy of approximately 0.2 eV, resulting in hydrogen storage of 17.95 wt% [3].

Moreover, boron elements can modify Li and Na adsorption sites in graphdiyne, with double-sided decorations exceeding bulk cohesive energies. The structures have estimated hydrogen uptake capacities of 8.81 wt% and 7.73 wt%, while maintaining thermodynamic stability [35].

A study explored the effects of nitrogen (N) and sulfur (S) doping, as well as N and S co-doping, on the structural and electrical properties of the GDY carbon structure. The investigation also involved evaluating the H_2 adsorption and storage capacities of these modified structures. The results demonstrated that the introduction of N and S dopants led to significant variations in the adsorption energies of H_2 molecules. Additionally, the study observed that charge injection had a notable impact on H_2 adsorption capacity. The findings suggest that N and S doping, both individually and in combination, can effectively enhance the H_2 storage capabilities of GDY nanosheets [36].

According to the aforementioned findings, the distinctive high π hybrid structure of GDY results in a uniform nanohole distribution, nonuniform electron distribution, excellent electrical conductivity, high electron mobility, tunable band gaps, and high chemical stability. These properties render graphdiyne a promising material for high-performance products and a potential solution for hydrogen storage.

In this study, we investigate the effects of individual nitrogen (N) and sodium (Na) atom doping and decoration on the electronic and structural properties of GDY. Furthermore, we explore the behavior of hydrogen adsorption on both pristine and modified GDY sheets, employing DFT-D2 calculations. Our investigation delves into various carbon types and adsorption sites within the GDY framework to pinpoint the optimal positions for N doping and Na decoration. Subsequently, we systematically introduce H_2 molecules to the stable structures and analyze the mean adsorption energy. To support these interactions, we utilize Hirshfeld charge analysis, PDOS (Partial Density of States), and band structure diagrams to observe charge transfer phenomena.

2. Computational methods

In this study, we optimized all configurations to investigate the impact of N-doping and Na-decoration on the hydrogen storage capacity of the GDY structure. Geometry optimization was carried out using the spin-polarized DFT method with the Perdew-Burke-Ernzerhof (PBE) functional for exchange-correlation energy at the Generalized Gradient Approximation (GGA) theory level [37].

For these calculations, we employed the DMol3 module [38] within the Materials Studio software, utilizing the DNP basis set. This basis set offers accuracy comparable to the 6-31G (d, p) basis set [39,40]. To account for dispersive intermolecular interactions and long-range Van der Waals forces, we applied the DFT-D2 method developed by Grimme [41,42].

A 2×2×1 supercell of the GDY unit cell was constructed, including a 20 Å vacuum space in the z-direction to prevent layer interactions. In the Brillouin zone, we employed a 7×7×1 gamma-centered Monkhorst-Pack mesh for k-grid sampling. No symmetry constraints were enforced during the geometry optimization process, and all atoms were allowed to relax.

To ensure accurate results, we set convergence tolerances as follows: energy tolerance of 10^{-5} Ha, maximum force tolerance of 2×10^{-3} Ha $Å^{-1}$, displacement tolerance of 5×10^{-3} Å, and a global orbital cut-off radius of 5.1 Å.

Additionally, we calculated various parameters such as the band structure, density of states (DOS), partial density of states (PDOS), charge density, and Hirshfeld (Mulliken) atomic charges to qualitatively and quantitatively explain the results.

The stability of doped GDY structures can be assessed by calculating the cohesive energy (E_{coh}) using the following equation:

$$E_{coh} = \frac{E_{D-GDY} - nE_C - mE_{dopant}}{n+m} \quad (1)$$

where $E_{D\text{-}GDY}$, E_C and E_{dopant} represent the total energy of the doped or decorated GDY structure with N or Na, isolated carbon, and dopant (N or Na) atoms, respectively. In this equation, n and m denote the numbers of carbon and dopant atoms in the modified GDY, respectively

The average adsorption energy (E_{ads}) and consecutive adsorption energy (E_s) per H_2 molecule were calculated using the following equations:

$$E_{ads} = \frac{E_{nH_2+D-GDY} - E_{D-GDY} - nE_{H_2}}{n} \quad (2)$$

$$E_s = E_{nH_2+D-GDY} - E_{(n-1)H_2+D-GDY} - E_{H_2} \quad (3)$$

In these equations, $E_{nH2+D-GDY}$ represents the total energy of the complex containing doped GDY and n H_2 molecules, $E_{(n-1)H2+D-GDY}$ is the total energy of the complex containing doped GDY and (n-1) H_2 molecules, E_{D-GDY} is the total energy of doped GDY, and E_{H2} represents the energy of an isolated H_2 molecule. Here, 'n' signifies the number of adsorbed hydrogen molecules. The adsorption energy of the *nth* H_2 molecule onto the previous structure is denoted as Es. When the value of this energy falls below 0.1 eV, it serves as a criterion to cease the addition of hydrogen. This threshold indicates that the adsorbent is not sufficiently suitable for the adsorption of the nth hydrogen molecule.

The hydrogen storage capacity is determined using the following equation:

$$H_2 \text{ storage capacity (wt\%)} = \frac{M_{H_2}}{M_{H_2}+M_{sheet}} \times 100 \quad (4)$$

where M_{H2} represents the mass of adsorbed H_2, and M_{sheet} represents the mass of the host material.

3. Results and discussion:

3.1. Assessment of the structural and electronic properties of pristine and modified-GDYs

Fig. 1 displays the top view of the GDY supercell. The lattice parameters employed in all calculations were determined as follows: a = b = 18.94 Å, c = 20 Å, α = β = 90°, and γ = 120°. The GDY structure exhibits a symmetric composition, comprising a sp^2-hybridized hexagonal carbon ring and six sp-hybridized acetylenic carbon chains [43]. The structure encompasses three distinct types of carbon atoms: C1 ($C_{sp2\text{-}sp2}$), C2 ($C_{sp2\text{-}sp}$), and C3 ($C_{sp\text{-}sp}$), each characterized by different hybridizations. The connection of these carbon variants results in the formation of four types of bonds, each with bond lengths measuring 1.435, 1.395, 1.236, and 1.340 Å. The 2×2 supercell of GDY comprises 72 carbon atoms. The findings indicate that this nanostructure exhibits a semiconductor nature with a band gap of 0.44 eV at the gamma point. It's important to note that different computational conditions in theoretical studies may yield varying values for the band gap [3,44]. Furthermore, the GDY system lacks inherent spin polarization or magnetism due to identical spin-up and spin-down bands. Consequently, the results from the GDY structure optimization are consistent with previous research findings [40,45].

Three types of non-equivalent carbon atoms were replaced with nitrogen atoms, and the resulting structures were subsequently optimized. Remarkably, the substitution of a nitrogen atom for the C2 carbon atom resulted in the formation of the most stable structure among the modified configurations, as indicated by its cohesive energy (E_{coh}) of -7.231 eV.

In the subsequent investigation of the impact of sodium (Na) metal decoration on the GDY structure, Na atoms were placed at different positions on the GDY plane (H1, H2, H3, and B) and at varying distances (d). As shown in Table 1, it becomes evident that when the Na atom is positioned directly on the GDY plane (d=0) at the H3 site, it results in the most stable decorated GDY structure, accompanied by an adsorption energy (E_{ads}) of -3.804 eV. Upon decorating the Na atom at various sites on the most stable N-doped GDY structure, it is discernible from Table 1 that the H3 site consistently exhibits the highest stability among the

simultaneously doped and decorated structures. The adsorption energy at the H3 site is recorded as -3.347 eV.

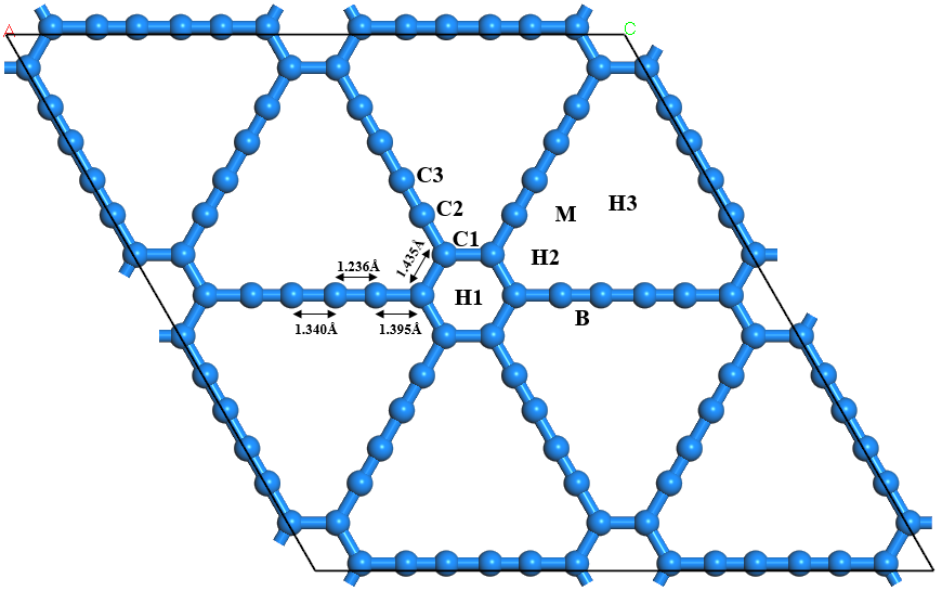

Fig. 1. The optimized structures of pristine GDY with various C-C bond lengths, three types of C atoms and five considered sites are labled as C1-C3 and H1-H3, B, and M, respectively.

Table 1. Binding energies and adsorption energies of modified GDYs (N doped, Na decorated, and N doped Na decorated) structures at different binding and adsorption sites.

Structure	Cohesive Energy (eV)			Adsorption energy(eV)						
	C1	C2	C3	H1		H2		H3		B
				d(Å)=0	d(Å)=1.5	d(Å)=0	d(Å)=1.5	d(Å)=0	d(Å)=1.5	d(Å)=1.5
N-GDY	-7.216	-7.231	-7.226	--	--	--	--	--	--	--
Na-GDY	--	--	--	-2.986	-2.963	-3.803	-3.802	-3.804	-3.797	-3.502
N, Na-GDY	--	-7.231	--	-2.759	-2.759	-3.346	-3.344	-3.347	-3.344	-3.334

In the subsequent sections of this paper, the most stable configurations of pure GDY, N-GDY, Na-GDY, and N, Na-GDY structures have been designated as S1, S2, S3, and S4, respectively. Table 2 presents the bond lengths, cohesive energies, bandgap energies (E_g), and Fermi levels (E_f) for these stable structures. The optimized geometrical structures are depicted in Fig. 2, providing both top and side views.

Table 2. Structural and electronic properties of pristine GDY and best conformations of the modified GDYs.

Structure	C1-C1 (Å)	C1-C2 (Å)	C2-C3 (Å)	C3-C3 (Å)	E_{coh} (eV)	E_{ads} (eV)	E_g (eV)	E_f (eV)
(S1)	1.236	1.395	1.435	1.340	-7.266	-	0.445	-5.223
(S2)	1.197	1.347	1.438	1.323	-7.231	-	0.000	-4.906
(S3)	1.239	1.394	1.435	1.339	-7.219	-3.804	0.000	-4.850
(S4)	1.209	1.339	1.439	1.315	-7.178	-3.347	0.000	-4.841

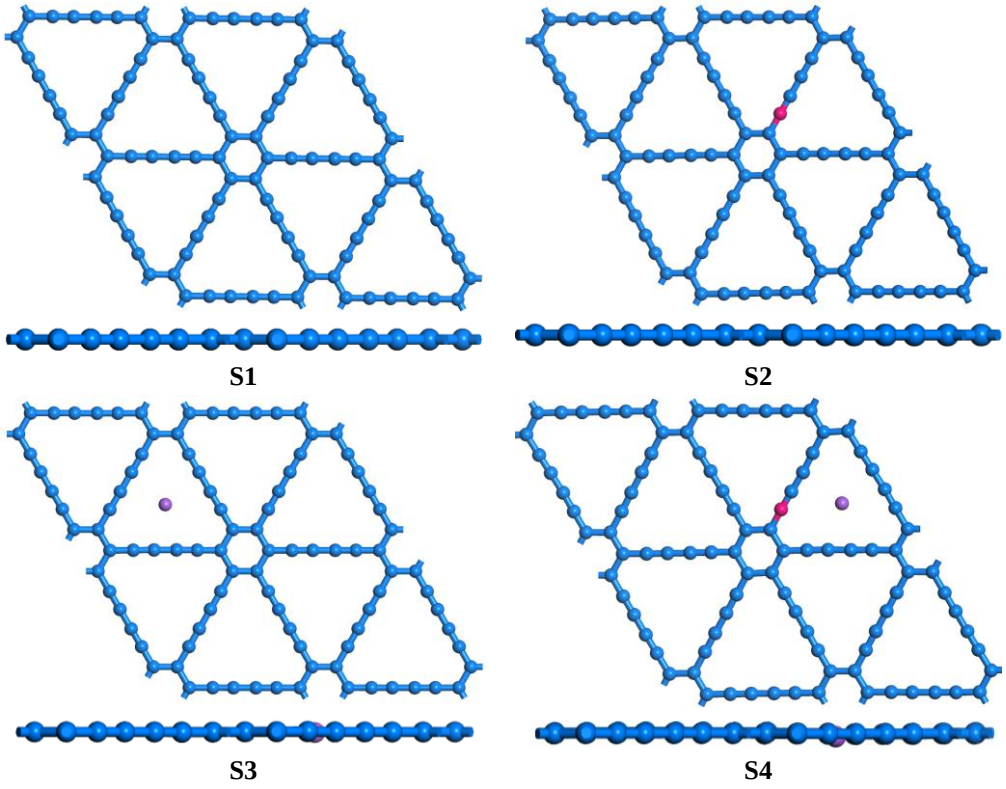

Fig. 2. The optimized geometrical structure of Pristine GDY (S1), N-GDY (S2), Na-GDY (S3), and N, Na-GDY (S4). (The blue, dark pink and purple balls represent C, N, and Na atoms, respectively.)

The introduction of nitrogen (N) into the GDY framework bri ngs about both structural and electronic effects. The smaller size of the N atom and its higher electronegativity in comparison to carbon (C) can induce changes in the bond lengths of neighboring atoms. As depicted in Table 2, there is a reduction in the lengths of C_{sp2}-C_{sp} and C_{sp}-C_{sp} bonds, accompanied by an increase in C_{sp2}-C_{sp2} bond length. The replacement of C with N results in the formation of N-C bonds, causing alterations in electron distribution, which, in turn, impacts the total energy of the structure.

The band structure diagrams for the S1-S4 structures are displayed in Fig. 3, with the Fermi level set at zero. Notably, the band gap of N-GDY undergoes a transformation, decreasing from 0.445 eV to zero. This transition signifies a shift from a semiconductor to a semi-metallic nature. The modification of the GDY structure results in an elevation of the Fermi level, moving closer to the conduction band. This observation suggests that the modified structures exhibit n-type semiconductor characteristics or improved semi-metallic properties, in alignment with prior reports for graphyne. The S4 structure exhibits the most notable shift in the Fermi level, confirming its higher conductivity compared to the other modified structures. While pure GDY displays characteristics of a direct semiconductor, the introduction of nitrogen (N-GDY) and sodium (Na-GDY) induces alterations in the electron band structure, resulting in a complete overlap of the conduction bands with the Fermi energy level.

The electrical conductance is exponentially related to the bandgap (E_{gap}), with conductivity increasing as E_{gap} decreases. The difference between the highest occupied molecular orbital (HOMO) and the lowest unoccupied molecular orbital (LUMO) can be used to estimate the E_{gap} value, which, in turn, is linked to electric conductance through the formula [46]:

$$\sigma \propto e^{\frac{-E_{gap}}{kT}} \quad (5)$$

where σ represents electrical conductance, k is Boltzmann's constant, and T denotes absolute temperature. This relationship highlights a fundamental aspect of semiconductor behavior: conductivity increases as the bandgap decreases. Lower band gaps result in higher conductance, a principle that is crucial in understanding the electrical properties of materials.

We have specifically applied this concept to our study on GDY. Our analysis (Table 2 and Fig. 3) reveals that GDY exhibits semiconductor behavior with a direct band gap of 0.445 eV at the gamma point (S1), a value consistent with recent research findings [40]. In modified GDY structures (S2, S3, and S4), alterations in the band gap are observed, leading to shifts in the

conduction bands relative to the Fermi level. This phenomenon results in a transformation of GDY from a semiconductor to a semi-metallic state.

Understanding the relationship between bandgap and electrical conductance is essential not only for characterizing materials like GDY but also for predicting their behavior under various conditions. For instance, in our study, we investigated the influence of hydrogen molecules during adsorption processes. Such insights are invaluable for the design and optimization of materials for specific applications where electrical conductivity is a critical factor.

In summary, the formula for electrical conductance provides a quantitative framework for elucidating the electronic properties of materials, thereby facilitating informed decision-making in material design and engineering.

In the S2 structure, Hirshfeld charges of neighboring N atoms, specifically C1 and C3, have undergone a significant change, transitioning from 0.023 e^- and 0.013 e^- to 0.062 e^- and 0.134 e^-, respectively. This shift indicates a transfer of electron density to the N atom, resulting in a Hirshfeld charge of -0.004 e^- for the N atom. Consequently, the introduction of the N atom disrupts the electric charge symmetry of the structure.

Furthermore, the presence of Na metal in the GDY structure induces charge transfer to the C atoms, with the Na atom carrying a positive charge of +0.482. In the S4 structure, the charge transfer from the Na metal to the electronegative N atom results in a more negative charge for the N atom compared to the S3 structure (refer to Fig. 4).

Figure 5 presents the Total Density of States (TDOS) and Projected Density of States (PDOS) diagrams for the S1 to S4 structures. Analyzing the Density of States (DOS) offers valuable insights into the bonding mechanisms, atom interactions, hybridization, and the effects of charge transfer.

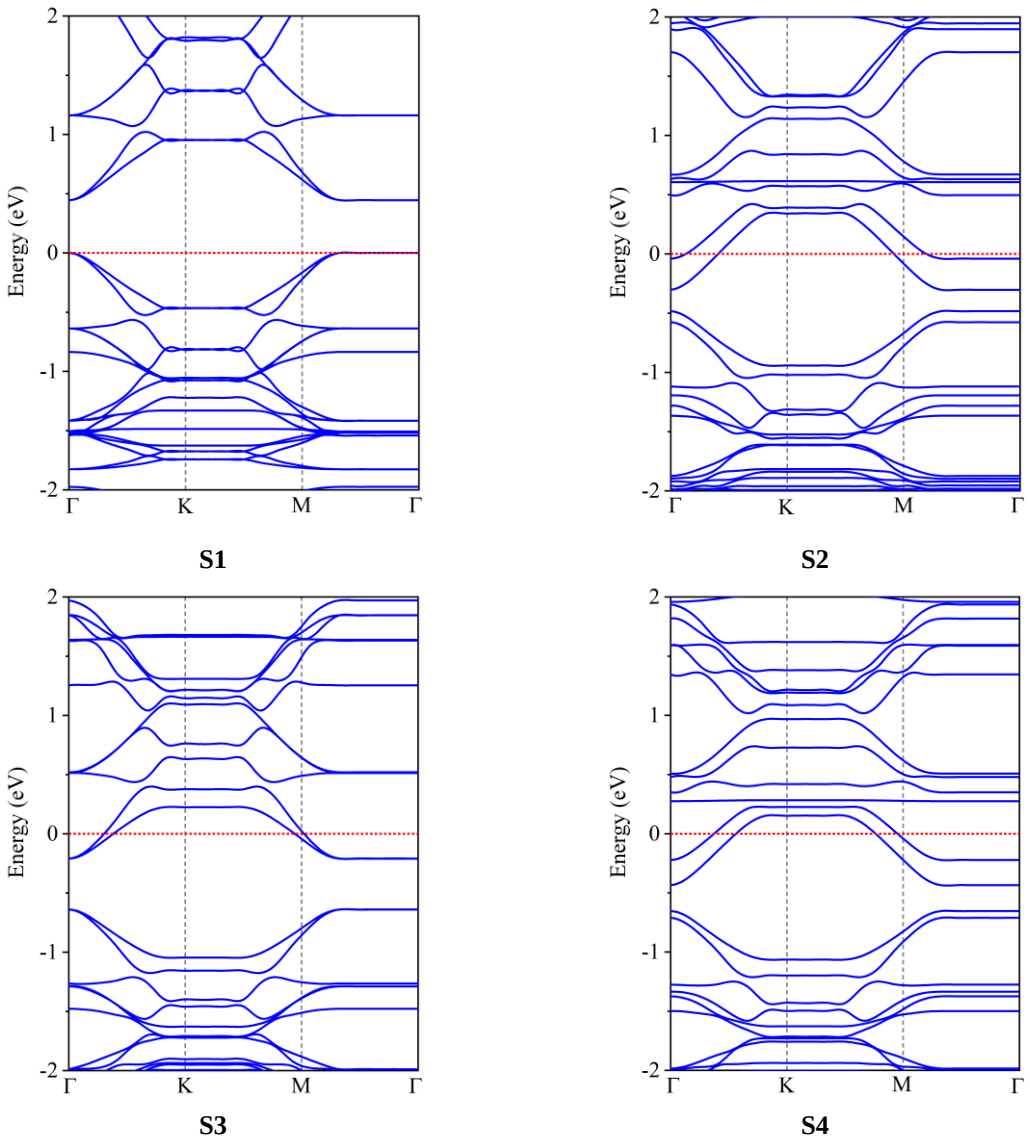

Fig. 3. Band structure of (S1) pristine GDY, (S2) N-GDY, (S3) Na-GDY and (S4) N, Na-GDY. The Fermi level was set to zero.

A comparison of the PDOS diagrams between pristine GDY (S1) and N-doped GDY (S2) reveals an increase in the contribution of s and p orbitals around the Fermi energy. This increase can be attributed to the higher number of electrons in the p orbital of the N atom introduced in the N-doped GDY structure. The introduction of N as an impurity enhances the electron density at energy levels above the Fermi level, which plays a crucial role in electrical conductivity and the transition of the structure from a semiconductor to a semi-metallic state.

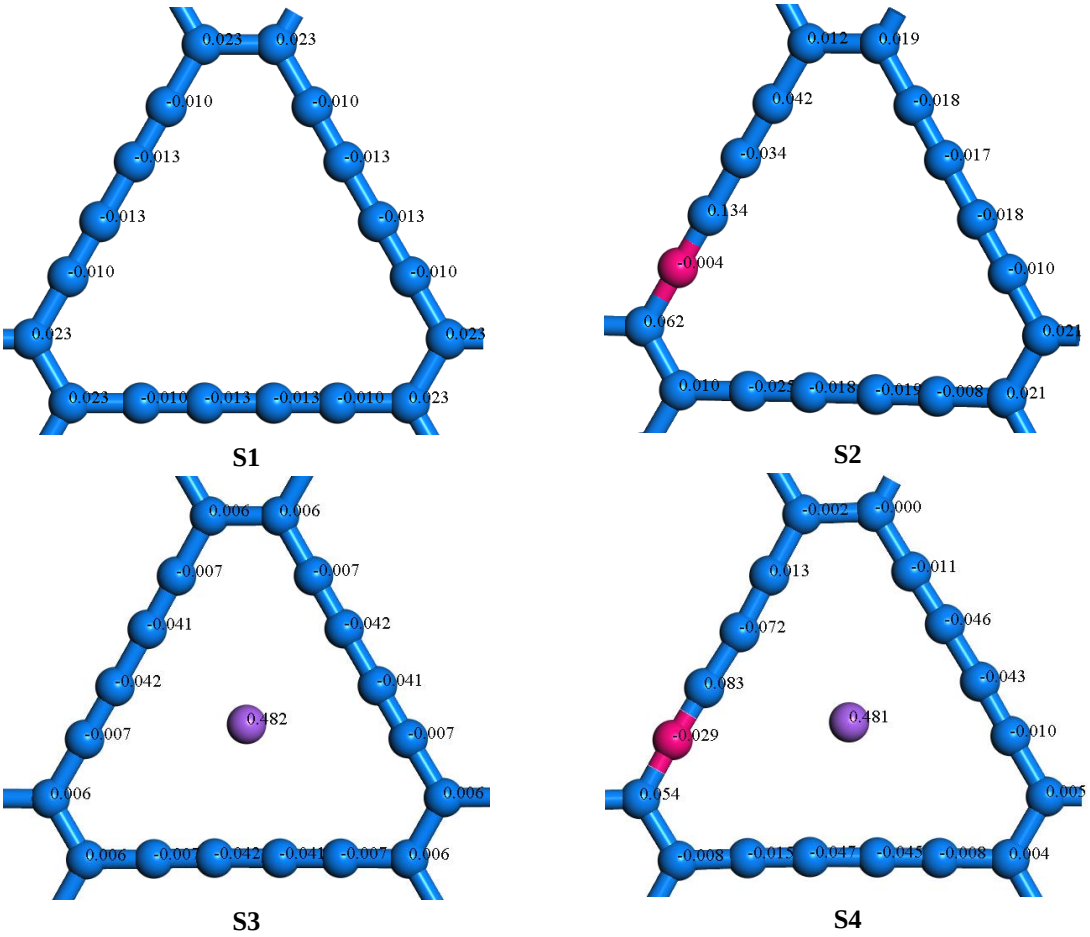

Fig. 4. Hirshfield charges of C, N, and Na atoms in pristine (S1), N-GDY (S2), Na-GDY (S3), and N, Na-GDY (S4).

The charge density distribution in the s orbital for GDY spans the energy range of -6 to -20 eV, while for N-doped GDY, it extends from -6 to -22 eV. Overall, in the N-doped GDY structure, there is a shift in electron density towards lower energy levels, and the transfer of electric charge from the N orbitals to the anti-bonding orbital of the carbon atoms leads to an increased charge density at energy levels above the Fermi level.

In the PDOS analysis of the S3 structure, the charge distribution and density within the s orbital remained relatively stable when compared to the pristine GDY structure. However, a notable shift in charge distribution towards higher energy levels occurred upon Na decoration.

Additionally, the charge distribution in the conduction band exhibited an increase in the decorated structure in contrast to the pristine GDY structure.

Within the S3 structure, the carbon atoms featuring sp^2-sp^2 hybridization displayed a decrease in charge density within the π orbital, while the charge density in the π* orbital increased. This observation is likely a result of charge transfer from the Na metal to this anti-bonding orbital. Furthermore, the charge density in the p and s orbitals of the C_{sp}-C_{sp} atom decreased, and the charge density distribution spanned a wider range of energy levels.

Analysis of the PDOS also revealed a low charge density in the Na orbitals, consistent with the anticipated electronic charge of the Na atom. Consequently, Na contributed additional electronic charge to the atoms of the GDY structure. The elevation of the Fermi level led to a downward shift in the conduction band, facilitating conduction within the structure.

By examining the TDOS and PDOS diagrams of the pristine GDY structure following the introduction of N and Na (S4), we can assess the combined effects. In the TDOS diagram, the p orbital displayed an increased charge density due to N doping. This implies that the presence of Na metal, akin to N doping, has led to an augmentation in the electron population within the p orbital at energy levels beyond the Fermi level.

When comparing the PDOS diagrams of carbon atoms, noticeable changes were observed. The π* orbital of the carbon atom featuring sp^2-sp hybridization exhibited the most significant alteration in charge density, while the π orbital of the C_{sp}-C_{sp} carbon atom experienced the highest increase. This observation suggests that the electric charge donated by Na metal atoms tends to accumulate in the bonded orbitals of C_{sp}-C_{sp} and non-bonded orbitals of C_{sp2}-C_{sp} carbon atoms.

In summary, the incorporation of N and Na into the GDY structure results in discernible effects. The TDOS diagram indicates an increase in charge density in the p orbital, signifying enhanced electron population above the Fermi level. Furthermore, the PDOS analysis reveals that the

charge density changes predominantly occur in the π* orbital of carbon atoms with sp^2-sp hybridization and the π orbital of C_{sp}-C_{sp} carbon atoms. These findings suggest that the electrical charge donated by Na metal atoms tends to be concentrated in specific carbon orbitals within the GDY structure.

3.2. Adsorption of single H_2 molecule onto the pristine and modified-GDYs

Subsequently, we proceeded to investigate the adsorption of a single H_2 molecule on both the pristine GDY (S1) and modified-GDY structures (S2, S3, and S4). We explored various positions around the nanosheets, both horizontally and vertically, and assessed the adsorption energy. Fig. 6 depicts the most stable configurations of H_2 adsorption on the pristine GDY and modified GDY structures. Table 3 provides the results concerning H_2 adsorption on different sites (H1, H2, H3, B, and M) of S1-S4 structures in both the vertical (V) and horizontal (H) directions.

It is noteworthy that the modified structures exhibited a greater capacity to adsorb H_2 compared to the pristine structure, indicating an enhancement in adsorption properties due to the introduced modifications. Among all the modified structures, the S2 structure displayed the most favorable adsorption properties, primarily due to its higher adsorption energy.

Table 3. Adsorption energy of single adsorbed H_2 on the pristine and the modified GDY at different considered sites.

Structure	Adsorption energy(eV)									
	H1		H2		H3		B		M	
	V	H	V	H	V	H	V	H	V	H
S1	-0.167	-0.187	-0.176	-0.166	-0.185	<u>-0.204</u>	-0.159	-0.161	--	--
S2	-0.131	-0.128	-0.126	-0.442	-0.133	<u>-0.455</u>	-0.111	-0.112	--	--
S3	-0.161	-0.148	-0.285	-0.287	-0.270	<u>-0.289</u>	-0.110	-0.184	--	--
S4	-0.153	-0.148	-0.283	-0.284	-0. 280	-0.281	-0.130	-0.148	-0.135	<u>-0.286</u>

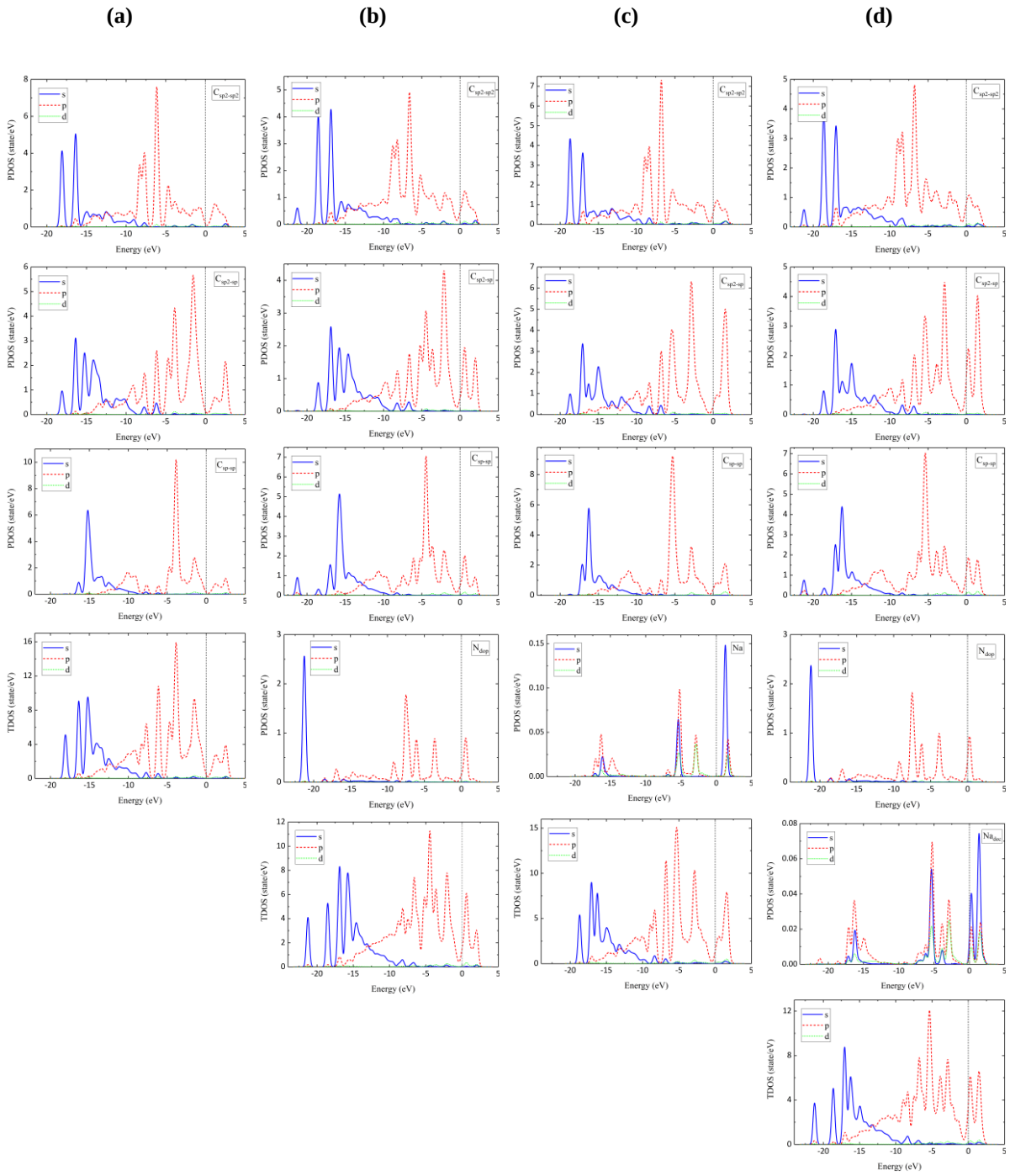

Fig. 5. TDOS and PDOS diagrams related to (a) S1, (b) S2, (c) S3, and (d) S4.

As indicated in Table 3, H3 emerges as the most favorable location for H_2 adsorption on structures S1, S2, and S3, while M proves to be the optimal adsorption site for S4, positioned between H3 and the C2 atom's location. Table 4 provides information on the adsorption energy, H-H bond length, and charge associated with each H, N, and Na atom for all systems.

The calculated bond length and angle for a free H_2 molecule stand at 0.748 Å and 180.0°, respectively. However, as the H_2 molecule adsorbs onto the S1-S4 structures, the H-H bond length experiences an increase, with the maximum value observed in the S4 structure at 0.752 Å.

Table 4. Adsorption energy (E_{ads}) of single adsorbed H_2, H–H bond length ($L_{H–H}$), and the charge of H in H_2 molecule, and the charges of N and Na atoms (e) in S1-S4 structures.

			Hirshfeld charges (e)			
Structure	E_{ads}	L_{H-H}	H	H	N	Na
S1	-0.204	0.751	-0.023	-0.021	-	-
S2	-0.455	0.751	-0.022	-0.014	-0.003	-
S3	-0.289	0.751	0.024	0.023	-	0.434
S4	-0.286	0.752	0.020	0.019	-0.028	0.436

Furthermore, in Fig. 7, the electrical charge distribution of each atom is depicted. It is clear that the electrical charge of the hydrogen molecule atoms varies across different structures, leading to energy variations and exerting an influence on the overall structural stability. This energy discrepancy arises from differences in Coulombic energy and subsequently affects the adsorption energy, consequently influencing the structural stability of the systems.

The PDOS diagrams in Fig. 8 provide insights into the interactions between hydrogen and the pristine and modified GDY structures. These diagrams illustrate the contribution of each type of structural carbon atom, modifier atoms (N, Na), and H_2 in various states. For the S1 structure, the PDOS reveals a weak interaction between the H_2 molecule and pristine GDY, which is consistent with observations in other structures [10,11]. This is primarily due to the low contribution of C atoms in the bonding orbitals around -5 eV.

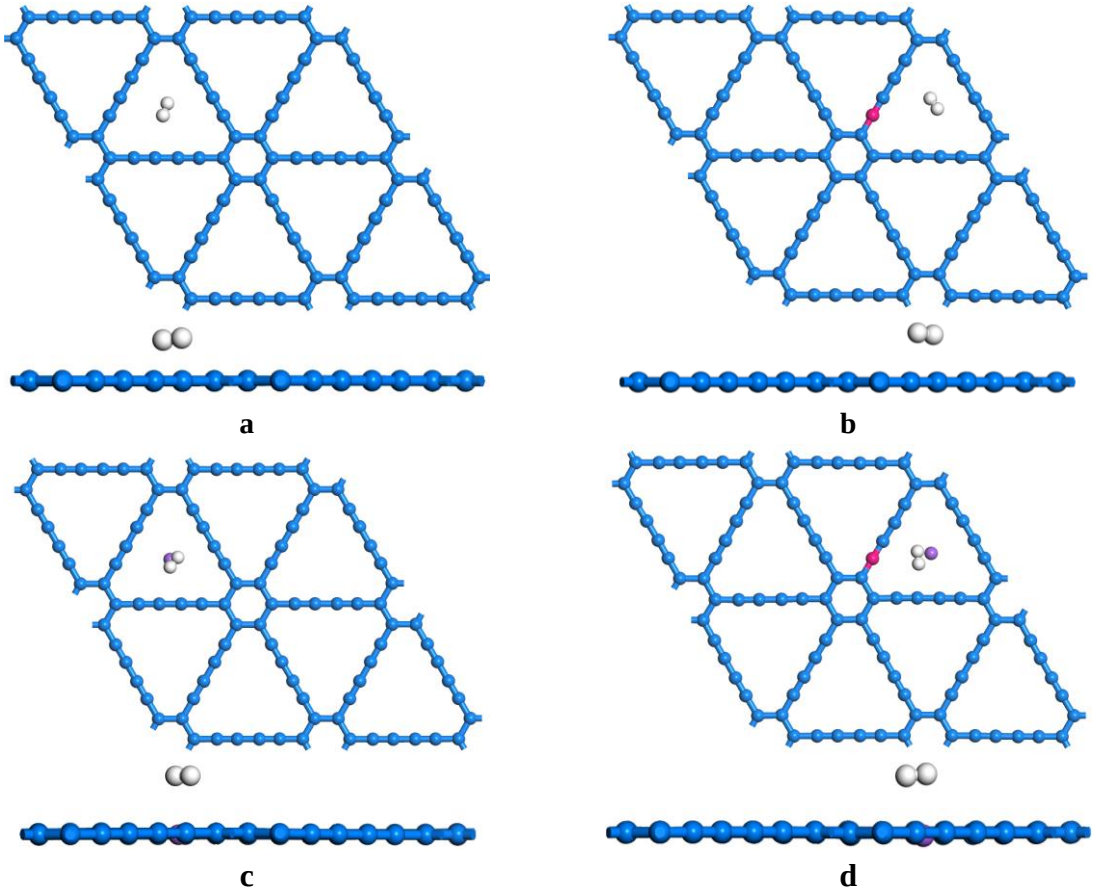

Fig. 6. Top and side views of the most stable sites and orientation of the H_2 adsorption on (a) S1, (b) S2, (c) S3, and (d) S4 structures.

In the case of the N-GDY system, when the C1 atom is replaced with N in the S2 and S4 structures, the PDOS diagram displays a noteworthy interaction between the N atom and the C atoms in the GDY sheet. Specifically, the peaks of the N atom and the p-orbitals of the GDY sheet's C atoms exhibit effective hybridization. This interaction is observed in the energy range of -4 to -8 eV, where the N(p) peaks align with the C(p) peaks, as well as in the vicinity of the Fermi level. As a result, a strong N-bond is formed within the GDY structure.

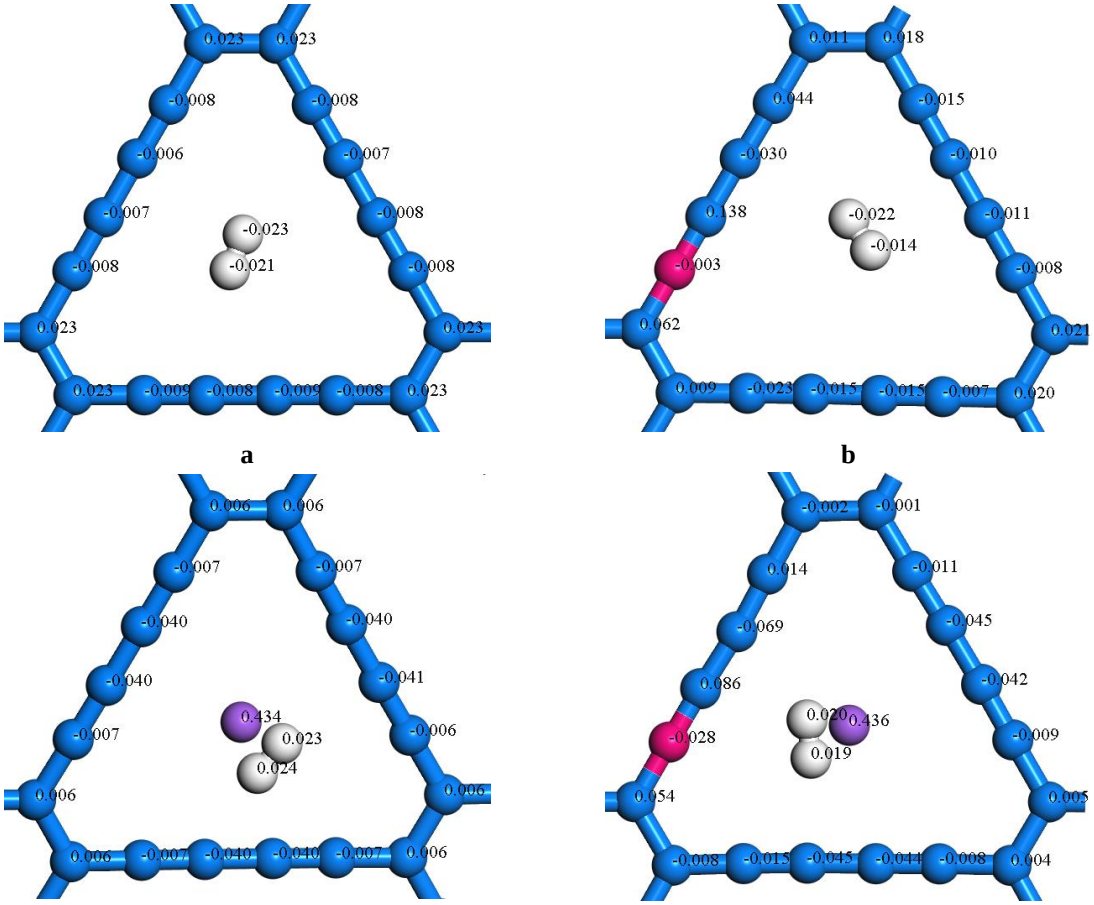

Fig. 7. The atomic Hirshfeld charges in the H_2 adsorbed structures: (a) S1 (b) S2, (c) S3, and (d) S4

Due to the N atom's surplus electrons compared to the C atom, the introduction of N into the GDY lattice leads to an increase in electron density within the valence band. This results in the presence of additional electron-filled states near the lower conduction bands, facilitating the easy transition of electrons into the conduction band. Essentially, the extra valence electron originating from the N atom's 2p orbital contributes to the GDY π* state.

In the PDOS diagrams, it becomes evident that the interaction between the N atom's p orbitals and the H_2 molecule is stronger compared to the interaction between the Na metal orbital and the H_2 molecule (between -5 to -10 eV) in S3 and S4 structures. As a result, the adsorption of the hydrogen molecule on the S2 structure is more pronounced than on the S3 and S4 structures. This is further supported by the adsorption energy value of -0.455 eV, confirming the stronger

interaction. Therefore, it can be concluded that the overlap of orbitals between the H_2 molecule and the adsorbent, observed in the PDOS of modified structures, can improve the adsorption of H_2 gas molecules.

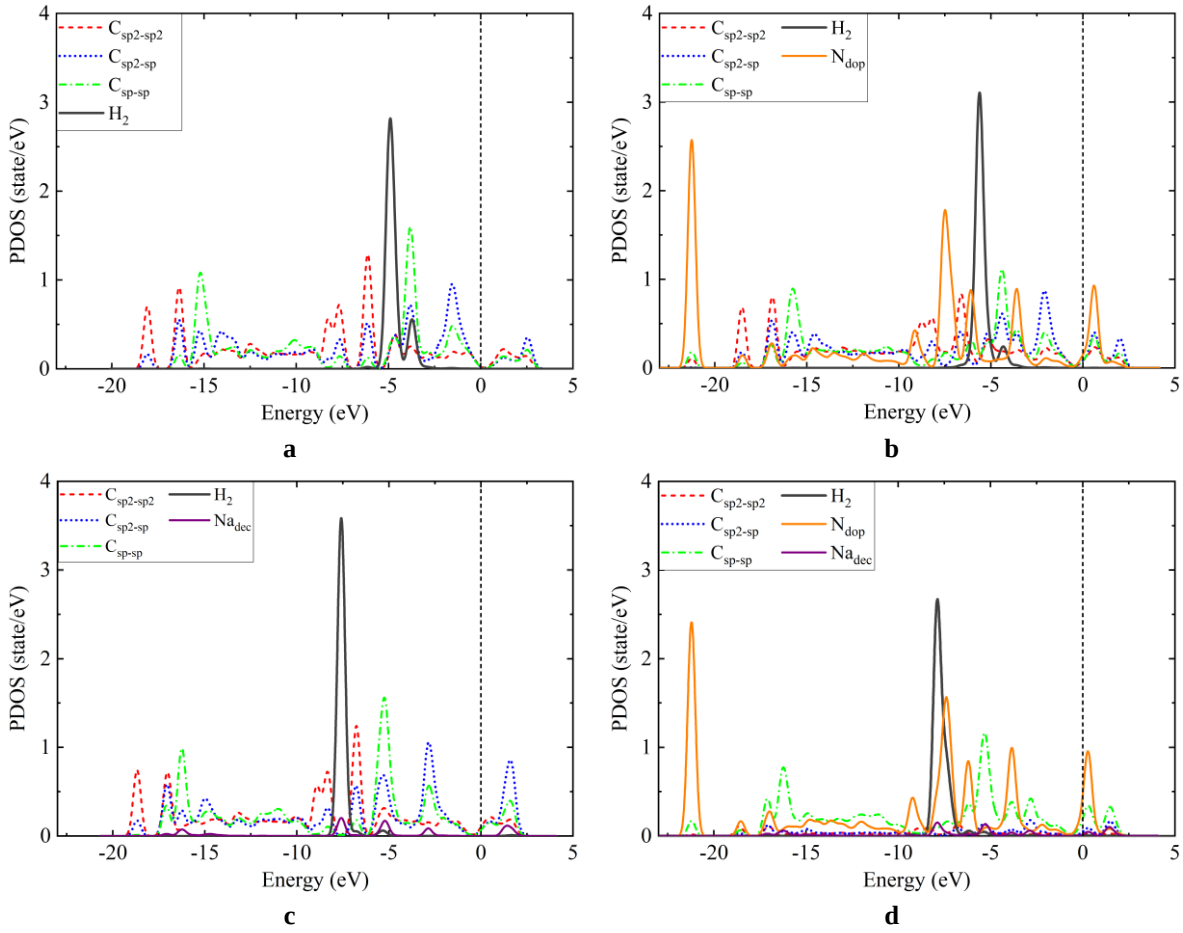

Fig. 8. The PDOS diagrams of the H_2 adsorbed onto: (a) S1, (b) S2, (c) S3, and (d) S4 structures.

Fig. 9 presents the electron density distribution for each structure, with yellow and red sections denoting depleted and enhanced electron areas, respectively. An intriguing observation is that the introduction of Na into the 18-ring structure results in the accumulation of electrons in a specific region. This electron accumulation has the potential to generate an electric field within the GDY structure, which could be a contributing factor to the enhanced performance of the S3 and S4 structures in terms of H_2 adsorption.

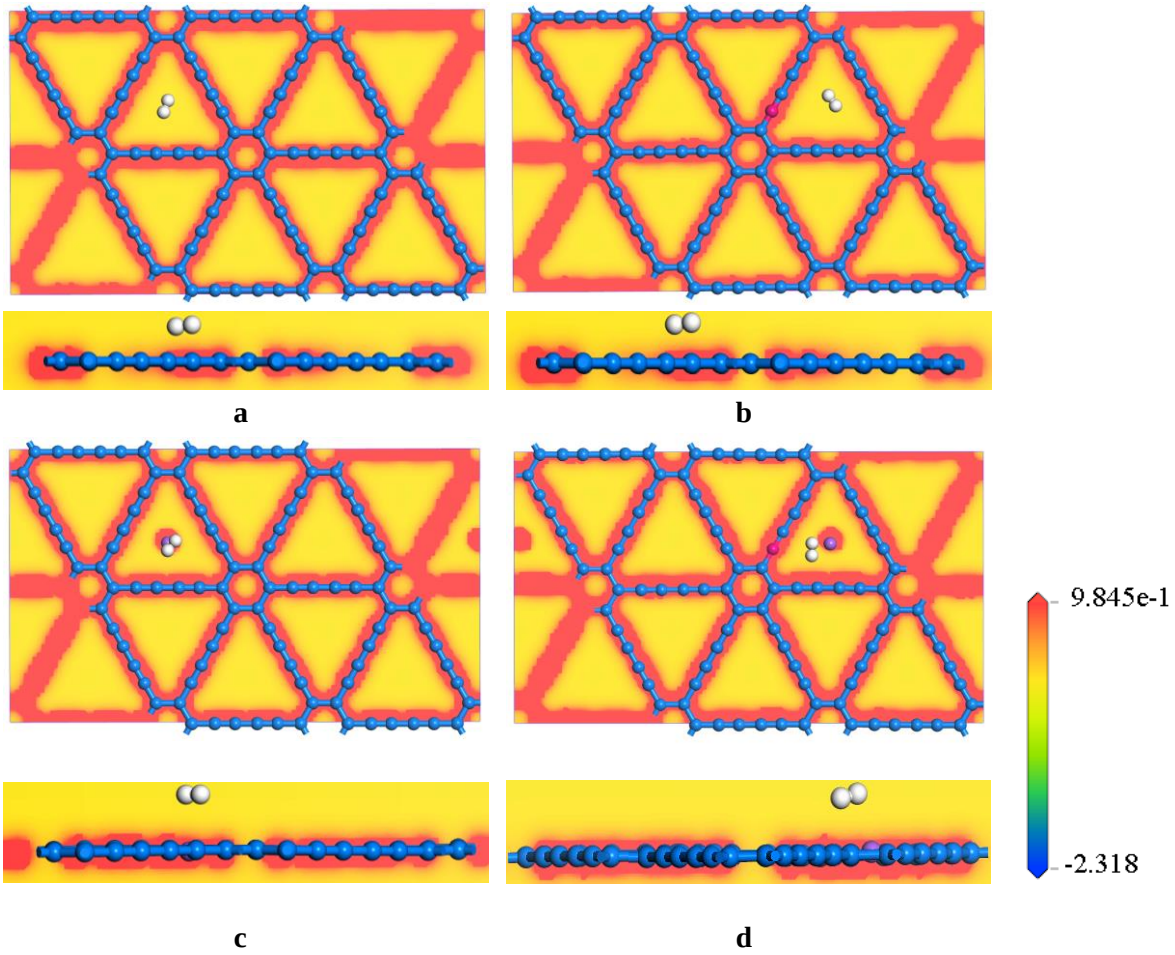

Fig. 9. The difference electron density images of adsorbed H_2 onto (a) S1, (b) S2, (c) S3, and (d) S4 structures.

3.3. Storage

To determine the optimal performance of a structure, hydrogen storage capacity plays a crucial role. To evaluate the maximum adsorption capacity of each structure, H_2 molecules were progressively added, and the systems were optimized at each step to obtain the total adsorption energy (E_{ads}) and the adsorption energy at each incremental addition (E_s). The United States Department of Energy has defined an optimal range for hydrogen uptake, which serves as a performance benchmark. Table 5 provides data on the average adsorption energy, adsorption energy at each incremental step, H-H bond length, and hydrogen storage capacity (wt%) for S1-S4 structures.

Initially, the bond length of the H_2 molecule measures 0.748 Å. However, as the process of hydrogen uptake and storage proceeds, the bond lengths of all H_2 molecules increase, falling within the range of 0.750 to 0.752 Å. The adsorption capacity of the H_2 molecule for structures S1, S2, S3, and S4 is found to be 4, 12, 19, and 19 H_2 molecules, respectively. In Fig. 10, the structures S1-S4 with maximum H_2 absorption are depicted.

The calculated weight percentages for structures S1, S2, S3, and S4 are determined as 3.59%, 9.98%, 13.80%, and 13.70%, respectively. These values are comparable to those reported in other studies involving modified structures [24,34,36]. The introduction of N atoms into the structure significantly enhances the storage capacity of H_2. Furthermore, the inclusion of Na in structures S1 and S2 results in a threefold increase in the adsorption capacity compared to that of S1. While structures S3 and S4 accommodate the same number of H_2 molecules, the higher weight of structure S4 results in a slightly lower weight percentage than that of structure S3. Consequently, it can be inferred that structure S3 exhibits greater storage efficiency, achieved simply by incorporating Na within GDY.

The introduction of Na atoms into the structure creates an electron accumulation zone, enhancing the electric field, in addition to the existing field in the pristine structure. This phenomenon influences the storage of H_2 molecules, leading to a higher accumulation of H_2 within the adsorption region. Fig. 11 provides a comparison between the average adsorption energy (in eV) and the number of adsorbed H_2 molecules for both pristine and modified GDY nanosheets.

Table 5. The average adsorption energy (E_{ads}), consecutive adsorption energy (Es), H-H bond length (L_{H-H}) and maximum H_2 adsorption capacity (wt. %) for various number of H_2 molecules and for S1-S4 configurations.

Struc.	#H_2	E_{ads}	E_s	L_{H-H}	Wt. %	Struc.	#H_2	E_{ads}	E_s	L_{H-H}	Wt. %	Struc.	#H_2	E_{ads}	E_s	L_{H-H}	Wt. %
S1	1	-0.204	-0.204	0.751		S3	1	-0.288	-0.287	0.751		S4	1	-0.286	-0.286	0.752	
	2	-0.190	-0.177	0.751			2	-0.288	-0.287	0.751			2	-0.288	-0.290	0.752	
	3	-0.170	-0.129	0.751			3	-0.237	-0.137	0.751			3	-0.273	-0.243	0.752	
	4	-0.159	-0.128	0.751	3.59%		4	-0.216	-0.152	0.751			4	-0.235	-0.123	0.751	
	5	-0.139	-0.059	0.751			5	-0.207	-0.170	0.751			5	-0.232	-0.220	0.750	
S2	1	-0.455	-0.289	0.751			6	-0.198	-0.151	0.751			6	-0.221	-0.164	0.750	
	2	-0.298	-0.287	0.751			7	-0.197	-0.195	0.751			7	-0.210	-0.142	0.750	
	3	-0.248	-0.137	0.751			8	-0.189	-0.133	0.751			8	-0.202	-0.150	0.750	
	4	-0.221	-0.152	0.751			9	-0.182	-0.129	0.750			9	-0.197	-0.155	0.751	
	5	-0.204	-0.170	0.752			10	-0.178	-0.133	0.751			10	-0.191	-0.134	0.751	
	6	-0.194	-0.151	0.751			11	-0.176	-0.162	0.751			11	-0.186	-0.144	0.751	
	7	-0.190	-0.195	0.751			12	-0.173	-0.138	0.751			12	-0.181	-0.123	0.751	
	8	-0.184	-0.133	0.751			13	-0.170	-0.134	0.750			13	-0.179	-0.154	0.751	
	9	-0.178	-0.129	0.752			14	-0.170	-0.171	0.751			14	-0.177	-0.154	0.751	
	10	-0.174	-0.133	0.751			15	-0.166	-0.113	0.751			15	-0.174	-0.131	0.750	
	11	-0.171	-0.162	0.750			16	-0.163	-0.111	0.751			16	-0.173	-0.150	0.751	
	12	-0.166	-0.138	0.750	9.98%		17	-0.160	-0.124	0.751			17	-0.169	-0.117	0.750	
	13	-0.160	-0.086	0.750			18	-0.158	-0.114	0.751			18	-0.170	-0.180	0.751	
							19	-0.156	-0.124	0.751	13.8%		19	-0.170	-0.169	0.751	13.7%
							20	-0.153	-0.096	0.750			20	-0.165	-0.067	0.748	

4. Conclusion

In this study, we thoroughly examined the H_2 adsorption capacity of a carbon structure through the introduction of specific modifications and a detailed analysis of their effects on the electrical and structural properties. Specifically, we implemented discrete modifications, namely N doping and Na decoration, at various locations on the GDY nanosheet. Impurities introduced into a material can exert a profound influence on its properties, and in the case of GDY, our study explored the effects of N doping and Na decoration, which introduced three distinct types of impurities into the structure.

By systematically optimizing these modifications, we identified the most favorable positions for each type of impurity, resulting in GDY structures that combined both decoration and doping impurities. Our investigations led us to the conclusion that substituting the N atom at the C2 position with sp hybridization yielded the most stable structure among the N-doped GDY configurations, with a binding energy of -7.231 eV. The addition of N atoms introduced

476 structural changes due to the smaller atomic radius of N compared to C and differences in
477 electronegativity between these atoms. These changes influenced bond lengths and
478 transformed the structure from a semiconductor to a semi-metallic material.

479

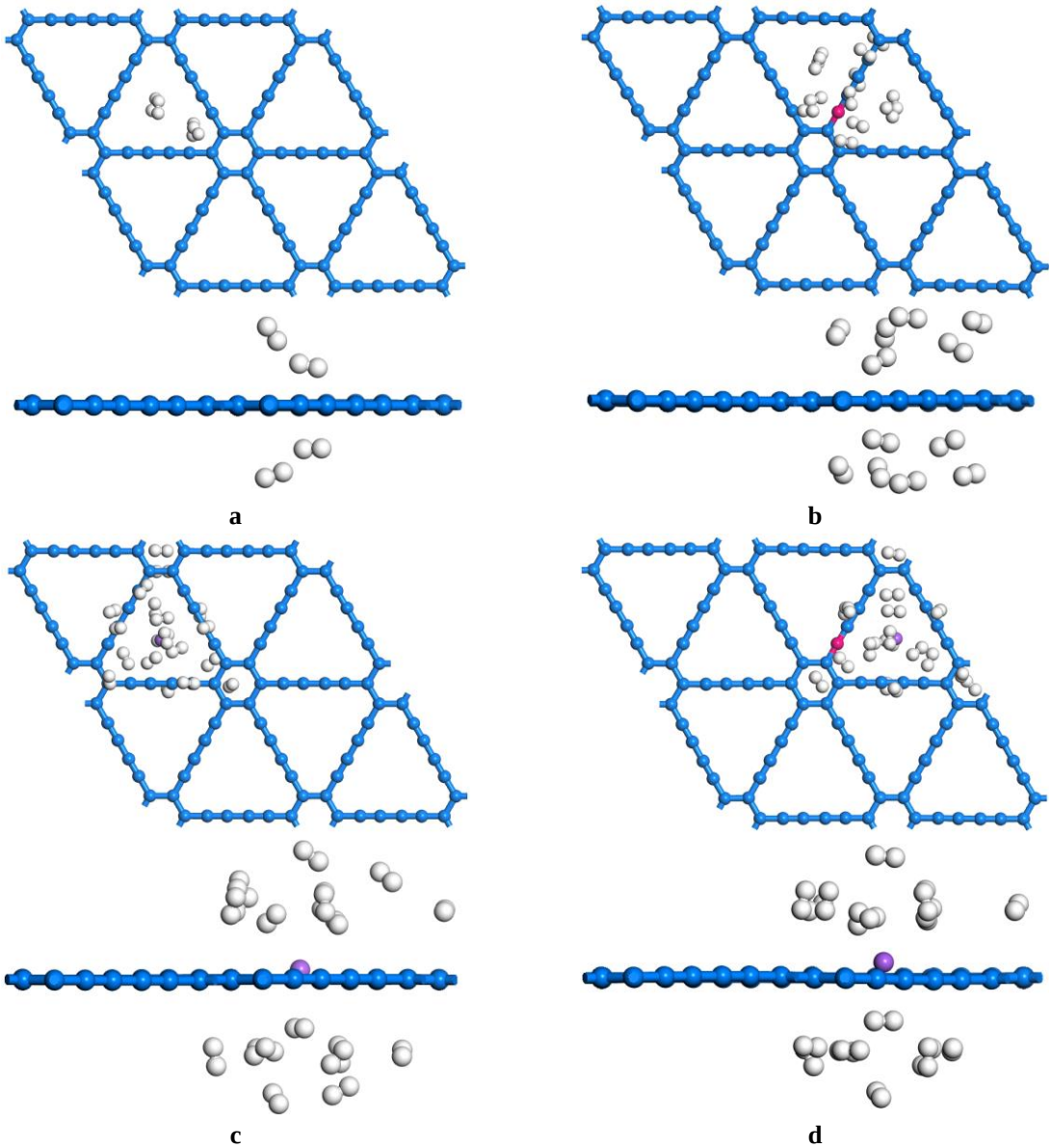

480 **Fig. 10**. Top and side views of the (a) $4H_2$/S1, (b) $12H_2$/S2, (C) $19H_2$/S3, and (d) $19H_2$/S4 structures

481

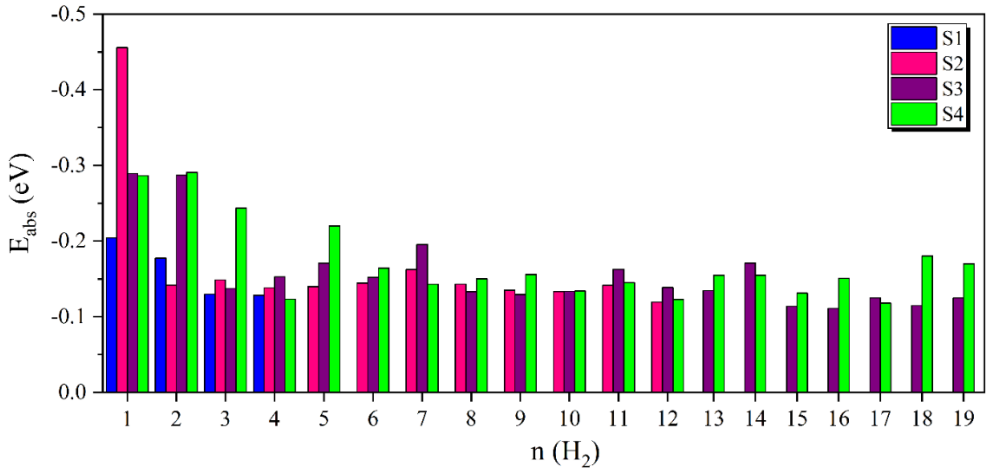

Fig. 11. The average adsorption energy (E_{ads}) of each step against the number of H_2 molecules adsorbed on S1-S4 structures.

Furthermore, the inclusion of Na atoms led to alterations in the charge distribution within the structure. The partial density of states (PDOS) diagrams revealed an increase in electronic states above the Fermi level, indicating enhanced conduction in Na-decorated GDY. We also explored the optimal sites for H_2 adsorption on both pristine and modified GDY structures, and our results indicated that the modified structures exhibited higher H_2 adsorption energies compared to the pristine structure. N-doped GDY displayed the highest H_2 adsorption energy, while the interaction between the H_2 molecule and the carbon atoms in the GDY structure remained limited, resulting in weaker binding.

According to the results, H3 is the best site for adsorption of H_2 on S1, S2, and S3, while M is the optimal site for H_2 adsorption on S4. The highest adsorption energy value observed was approximately 40 $kJ.mol^{-1}$, indicating that Van der Waals forces primarily drive the adsorption of H_2 on the nanosheets and is a physical adsorption [47].

Additionally, we investigated the maximum H_2 adsorption capacity for each structure by incrementally adding H_2 molecules. The results of this section show that the H_2 adsorption capabilities of S3 (Na-doped GDY) and S4 (N, Na-GDY) are almost three times more than S1

(pristine GDY). The S1, S2, S3, and S4 structures demonstrated the capacity to adsorb up to 4, 12, 19, and 19 H_2 molecules, with average adsorption energies of -0.159, -0.166, -0.156, and -0.170 eV per H_2, respectively. Notably, the Na-decorated GDY structure, S3, exhibited the highest H_2 storage capacity, reaching 13.8 wt%. This theoretical investigation highlights the potential of modified GDY nanosheets for hydrogen storage applications. It also points out promising prospects for improving H_2 adsorption capacity, storage, and detection through modifying the carbon structure.

Acknowledgments

M. A.B. and Z. B. would like to extend their sincere appreciation to the Research Council of Lorestan University.

References

[1] M. Song, Y. Chen, X. Liu, W. Xu, Y. Zhao, M. Zhang, C. Zhang, A first-principles study of gas molecule adsorption on hydrogen-substituted graphdiyne, Phys. Lett. A 384 (2020) 126332.

[2] P. Panigrahi, A.K. Dhinakaran, S.R. Naqvi, S.R. Gollu, R. Ahuja, T. Hussain, Light metal decorated graphdiyne nanosheets for reversible hydrogen storage, Nanotechnology 29 (2018) 355401. https://doi.org/10.1088/1361-6528/AAC84C.

[3] M. Ebadi, A. Reisi-Vanani, F. Houshmand, P. Amani, Calcium-decorated graphdiyne as a high hydrogen storage medium: Evaluation of the structural and electronic properties, Int. J. Hydrogen Energy 43 (2018) 23346–23356. https://doi.org/10.1016/J.IJHYDENE.2018.10.205.

[4] E. Klontzas, E. Tylianakis, G.E. Froudakis, Designing 3D COFs with enhanced

hydrogen storage capacity, Nano Lett. 10 (2010) 452–454. https://doi.org/10.1021/nl903068a.

[5] Z.Y. Zhong, Z.T. Xiong, L.F. Sun, J.Z. Luo, P. Chen, X. Wu, J. Lin, K.L. Tan, Nanosized Nickel(or Cobalt)/Graphite Composites for Hydrogen Storage, J. Phys. Chem. B 106 (2002) 9507–9513. https://doi.org/10.1021/JP020151J.

[6] O. Faye, J.A. Szpunar, An Efficient Way to Suppress the Competition between Adsorption of H 2 and Desorption of n H 2 -Nb Complex from Graphene Sheet: A Promising Approach to H_2 Storage, J. Phys. Chem. C 122 (2018) 28506–28517. https://doi.org/10.1021/acs.jpcc.8b09498.

[7] J. Kang, Z. Wei, J. Li, Graphyne and Its Family: Recent Theoretical Advances, ACS Appl. Mater. Interfaces 11 (2019) 2692–2706. https://doi.org/10.1021/acsami.8b03338.

[8] G.K. Dimitrakakis, E. Tylianakis, G.E. Froudakis, Pillared graphene: a new 3-D network nanostructure for enhanced hydrogen storage, Nano Lett. 8 (2008) 3166–3170. https://doi.org/10.1021/nl801417w.

[9] R. Matsuoka, R. Sakamoto, K. Hoshiko, S. Sasaki, H. Masunaga, K. Nagashio, H. Nishihara, Crystalline Graphdiyne Nanosheets Produced at a Gas/Liquid or Liquid/Liquid Interface, J. Am. Chem. Soc. 139 (2017) 3145–3152. https://doi.org/10.1021/jacs.6b12776.

[10] C. Tang, X. Zhang, The hydrogen storage capacity of Sc atoms decorated porous boron fullerene B40: A DFT study, Int. J. Hydrogen Energy 41 (2016) 16992–16999. https://doi.org/10.1016/J.IJHYDENE.2016.07.118.

[11] S. Yang, Z. Lan, H. Xu, G. Lei, W. Xie, Q. Gu, A First-Principles Study on Hydrogen Sensing Properties of Pristine and Mo-Doped Graphene, J. Nanotechnol. 2018 (2018). https://doi.org/10.1155/2018/2031805.

[12] M. Asgari Bajgirani, Z. Biglari, M. Sahihi, Computational investigation on CO2

capturing capacity of N-doped and Na-decorated Graphdiyne, Fuel 345 (2023) 128169. https://doi.org/10.1016/J.FUEL.2023.128169.

[13] Z. Tabandeh, A. Reisi-Vanani, Manipulation of the CO2 capture capability of graphdiyne using transition metal decoration and charge injection: A DFT-D2 study, Fuel 333 (2023) 126295. https://doi.org/10.1016/J.FUEL.2022.126295.

[14] M. Jiang, J. Xu, P. Munroe, Z.H. Xie, Z. Chen, Light metal decorated graphene-like Si2BN monolayers as hydrogen storage media: A DFT investigation, Int. J. Hydrogen Energy 50 (2024) 865–878. https://doi.org/10.1016/J.IJHYDENE.2023.08.174.

[15] S.K. Tiwari, S.K. Pandey, R. Pandey, N. Wang, M. Bystrzejewski, Y.K. Mishra, Y. Zhu, Stone–Wales Defect in Graphene, Small 19 (2023) 2303340. https://doi.org/10.1002/SMLL.202303340.

[16] Z.J. Li, F.F. Wang, Z.R. Li, H.L. Xu, X.R. Huang, D. Wu, W. Chen, G.T. Yu, F.L. Gu, Y. Aoki, Large static first and second hyperpolarizabilities dominated by excess electron transition for radical ion pair salts M2˙+TCNQ˙− (M = Li, Na, K), Phys. Chem. Chem. Phys. 11 (2009) 402–408. https://doi.org/10.1039/B809161G.

[17] M. Kurban, İ. Muz, Theoretical investigation of the adsorption behaviors of fluorouracil as an anticancer drug on pristine and B-, Al-, Ga-doped C36 nanotube, J. Mol. Liq. 309 (2020) 113209. https://doi.org/10.1016/J.MOLLIQ.2020.113209.

[18] H. Kurban, S. Alaei, M. Kurban, Effect of Mg content on electronic structure, optical and structural properties of amorphous ZnO nanoparticles: A DFTB study, J. Non. Cryst. Solids 560 (2021) 120726. https://doi.org/10.1016/J.JNONCRYSOL.2021.120726.

[19] İ. Muz, M. Kurban, A first-principles evaluation on the interaction of 1,3,4-oxadiazole with pristine and B-, Al-, Ga-doped C60 fullerenes, J. Mol. Liq. 335 (2021) 116181. https://doi.org/10.1016/J.MOLLIQ.2021.116181.

[20] M.Kurban, Sulfur doping concentration effect on the electronic and structural properties

of ZnO nanoparticles: Insights from DFTB calculations, Comput. Theo. Chem. 1224, 114112. https://doi.org/10.1016/j.comptc.2023.114112

[21] F.J. Isidro-Ortega, J.H. Pacheco-Sánchez, A. González-Ruíz, R. Alejo, DFT study of hydrogen storage on the metallic decoration of boron substitution on zeolite templated carbon vacancy, Int. J. Hydrogen Energy 45 (2020) 19505–19515. https://doi.org/10.1016/J.IJHYDENE.2020.05.017.

[22] C. Xiang, A. Li, S. Yang, Z. Lan, W. Xie, Y. Tang, H. Xu, Z. Wang, H. Gu, Enhanced hydrogen storage performance of graphene nanoflakes doped with Cr atoms: a DFT study, RSC Adv. 9 (2019) 25690–25696. https://doi.org/10.1039/C9RA04589A.

[23] P.P. Liu, H. Zhang, X.L. Cheng, Y.J. Tang, External electric field: An effective way to prevent aggregation of Mg atoms on γ-graphyne for high hydrogen storage capacity, Appl. Surf. Sci. 371 (2016) 44–49. https://doi.org/10.1016/J.APSUSC.2016.02.223.

[24] F. Akbari, A. Reisi-Vanani, M.H. Darvishnejad, DFT study of the electronic and structural properties of single Al and N atoms and Al-N co-doped graphyne toward hydrogen storage, Appl. Surf. Sci. 488 (2019) 600–610. https://doi.org/10.1016/J.APSUSC.2019.05.272.

[25] G. Li, Y. Li, H. Liu, Y. Guo, Y. Li, D. Zhu, Architecture of graphdiyne nanoscale films, Chem. Commun. 46 (2010) 3256–3258. https://doi.org/10.1039/B922733D.

[26] X. Gao, H. Liu, D. Wang, J. Zhang, Graphdiyne: synthesis, properties, and applications, Chem. Soc. Rev. 48 (2019) 908–936. https://doi.org/10.1039/C8CS00773J.

[27] C. Sun, D.J. Searles, Lithium storage on graphdiyne predicted by DFT calculations, J. Phys. Chem. C 116 (2012) 26222–26226. https://doi.org/10.1021/jp309638z.

[28] S. Wang, L. Yi, J.E. Halpert, X. Lai, Y. Liu, H. Cao, R. Yu, D. Wang, Y. Li, A Novel and Highly Efficient Photocatalyst Based on P25–Graphdiyne Nanocomposite, Small 8 (2012) 265–271. https://doi.org/10.1002/SMLL.201101686.

600 [29] Y. Jiao, A. Du, S.C. Smith, Z. Zhu, S.Z. Qiao, H2 purification by functionalized
601 graphdiyne – role of nitrogen doping, J. Mater. Chem. A 3 (2015) 6767–6771.
602 https://doi.org/10.1039/C5TA01062D.
603 [30] Z. Tabandeh, A. Reisi-Vanani, Investigation of the adsorption behavior of two
604 anticancer drugs on the pristine and BN-doped graphdiyne nanosheet: A DFT-D3
605 perception, Diam. Relat. Mater. 119 (2021) 108564.
606 https://doi.org/10.1016/J.DIAMOND.2021.108564.
607 [31] S. Zhang, H. Du, J. He, C. Huang, H. Liu, G. Cui, Y. Li, Nitrogen-Doped Graphdiyne
608 Applied for Lithium-Ion Storage, ACS Appl. Mater. Interfaces 8 (2016) 8467–8473.
609 https://doi.org/10.1021/acsami.6b00255.
610 [32] A.H. Farokh Niaei, T. Hussain, M. Hankel, D.J. Searles, Sodium-intercalated bulk
611 graphdiyne as an anode material for rechargeable batteries, J. Power Sources 343 (2017)
612 354–363. https://doi.org/10.1016/J.JPOWSOUR.2017.01.027.
613 [33] T. Hussain, B. Mortazavi, H. Bae, T. Rabczuk, H. Lee, A. Karton, Enhancement in
614 hydrogen storage capacities of light metal functionalized Boron–Graphdiyne
615 nanosheets, Carbon N. Y. 147 (2019) 199–205.
616 https://doi.org/10.1016/J.CARBON.2019.02.085.
617 [34] M. Dehkhodaei, A. Reisi-Vanani, The effect of the electric field intensity on the
618 hydrogen storage of B/N-co-doped graphdiyne nanosheet, Int. J. Hydrogen Energy 47
619 (2022) 36886–36897. https://doi.org/10.1016/J.IJHYDENE.2022.08.251.
620 [35] Y. Wang, G. Xu, S. Deng, Q. Wu, Z. Meng, X. Huang, L. Bi, Z. Yang, R. Lu, Lithium
621 and sodium decorated graphdiyne as a candidate for hydrogen storage: First-principles
622 and grand canonical Monte Carlo study, Appl. Surf. Sci. 509 (2020) 144855.
623 https://doi.org/10.1016/J.APSUSC.2019.144855.
624 [36] M. Dehkhodaei, A. Reisi-Vanani, Effect of the charge injection and N and S co-doping

on the structural and electronic properties, and hydrogen storage capacity of graphdiyne 2D structure, Surfaces and Interfaces 31 (2022) 102031. https://doi.org/10.1016/J.SURFIN.2022.102031.

[37] J.P. Perdew, K. Burke, M. Ernzerhof, Generalized Gradient Approximation Made Simple, Phys. Rev. Lett. 77 (1996) 3865. https://doi.org/10.1103/PhysRevLett.77.3865.

[38] B. Delley, From molecules to solids with the DMol3 approach, J. Chem. Phys. 113 (2000) 7756–7764. https://doi.org/10.1063/1.1316015.

[39] B. Delley, Hardness conserving semilocal pseudopotentials, Phys. Rev. B 66 (2002) 155125. https://doi.org/10.1103/PhysRevB.66.155125.

[40] X. Liu, Z. Wang, Y. Tian, J. Zhao, Graphdiyne-Supported Single Iron Atom: A Promising Electrocatalyst for Carbon Dioxide Electroreduction into Methane and Ethanol, J. Phys. Chem. C 124 (2020) 3722–3730. https://doi.org/10.1021/acs.jpcc.9b11649.

[41] S. Grimme, Semiempirical GGA-type density functional constructed with a long-range dispersion correction, J. Comput. Chem. 27 (2006) 1787–1799. https://doi.org/10.1002/JCC.20495.

[42] S. Grimme, J. Antony, S. Ehrlich, H. Krieg, A consistent and accurate ab initio parametrization of density functional dispersion correction (DFT-D) for the 94 elements H-Pu, J. Chem. Phys. 132 (2010). https://doi.org/10.1063/1.3382344/926936.

[43] Y. Fang, Y. Liu, L. Qi, Y. Xue, Y. Li, 2D graphdiyne: an emerging carbon material, Chem. Soc. Rev. 51 (2022) 2681–2709. https://doi.org/10.1039/D1CS00592H.

[44] F. He, Basic Structure and Band Gap Engineering: Theoretical Study of GDYs, Graphdiyne Fundam. Appl. Renew. Energy Electron. (2021) 13–77. https://doi.org/10.1002/9783527828470.CH2.

[45] X. Liu, W. Tang, S. Liu, X. Chen, Y. Li, X. Hu, L. Qiao, Y. Zeng, CO oxidation on Ni

and Cu embedded graphdiyne as efficient noble metal-free catalysts: A first-principles density-functional theory investigation, Appl. Surf. Sci. 539 (2021) 148287. https://doi.org/10.1016/J.APSUSC.2020.148287.

[46] Sheng S. Li, Semiconductor Physical Electronics (second ed.), Springer, New York (2006).

[47] V.J. Inglezakis, A.A. Zorpas, Heat of adsorption, adsorption energy and activation energy in adsorption and ion exchange systems, Desalin. Water Treat. 39 (2012) 149–157. https://doi.org/10.1080/19443994.2012.669169.